

Discovery of Mono- and Disubstituted 1*H*-Pyrazolo[3,4]pyrimidines and 9*H*-Purines as Catalytic Inhibitors of Human DNA Topoisomerase II α

Barbara Pogorelčnik,^[a] Matjaž Brvar,^[a] Bojana Žegura,^[b] Metka Filipič,^[b] Tom Solmajer,^[a] and Andrej Perdih^{*[a]}

Human DNA topoisomerase II α (htII α) is a validated target for the development of anticancer agents. Based on structural data regarding the binding mode of AMP-PNP (5'-adenylyl- β , γ -imidodiphosphate) to htII α , we designed a two-stage virtual screening campaign that combines structure-based pharmacophores and molecular docking. In the first stage, we identified several monosubstituted 9*H*-purine compounds and a novel class of 1*H*-pyrazolo[3,4]pyrimidines as inhibitors of htII α . In the second stage, disubstituted analogues with improved cellular activities were discovered. Compounds from both classes

were shown to inhibit htII α -mediated DNA decatenation, and surface plasmon resonance (SPR) experiments confirmed binding of these two compounds on the htII α ATPase domain. Proposed complexes and interaction patterns between both compounds and htII α were further analyzed in molecular dynamics simulations. Two compounds identified in the second stage showed promising anticancer activities in hepatocellular carcinoma (HepG2) and breast cancer (MCF-7) cell lines. The discovered compounds are suitable starting points for further hit-to-lead development in anticancer drug discovery.

Introduction

Targeted cancer therapy has been an interesting approach to treat different types of cancer. Human DNA topoisomerase is one of the major anticancer targets, due its role in cell proliferative process.^[1] Based on their mechanisms of action, DNA topoisomerases are classified into two groups: type I and type II. Type I acts by generating a transient single-stranded break in the DNA molecule, whereas type II catalyzes topological changes by breaking one double-stranded DNA segment, transporting another double-stranded DNA through the break, and finally, resealing the break.^[2–4] Thus far, many compounds with topoisomerase inhibitory activity have been successfully used in clinical practice for the treatment of various neoplasms.^[5,6] Inhibitors of human topoisomerase II α (htII α) are generally classified into two groups, which vary extensively in their mechanisms of action. Poisons (group I) act by stabilizing a transient covalent DNA–enzyme complex, thereby causing damage to the DNA molecule. The catalytic inhibitors (group II) interfere with a single step of the topo II catalytic cycle.^[4] To date, many compounds with topoisomerase inhibitory activity, such as epipodophyllotoxins^[7] (etoposide (1) and teniposide), anthracyclines^[8] (doxorubicin, daunorubicin, and mitoxan-

trone), and aminoacridine^[9] (amsacrine) have been used for cancer therapy. However, the low selectivity and high toxicity of these inhibitors resulted in the urgent need for novel and more efficient inhibitors of topo II α .^[1] Catalytic inhibitors (group II) are extremely structurally diverse compounds with different mechanisms of action. For example, aclarubicin and suramine prevent binding between DNA and topoisomerase II α ,^[10,11] merbarone prevents DNA cleavage,^[12] bisdioxipiperazine (e.g., compound ICRF-187) derivatives inhibit ATP hydrolysis,^[13] and purine analogues (e.g., compounds 2 and 3) inhibit ATP binding.^[14] In our previous work, we focused some of our research efforts on the bacterial analogue of topo II α , DNA gyrase, and successfully identified several novel classes of inhibitors targeting the ATP binding site located at its B subunit.^[15–17]

Based on the homology with bacterial DNA gyrase, it was proposed that htII α is composed of an N-terminal fragment, a central domain, and a C-terminal fragment. The first fragment (the N terminus) includes two domains: the ATPase domain, which is important for binding and hydrolysis of the ATP molecule, and the second, named a transducer domain.^[3,18] The ATPase domain of topoisomerase II α belongs to the GHKL superfamily, which includes enzymes such as DNA gyrase, Hsp90, histidine kinase, and MutL proteins.^[19,20] The second domain (central domain) is also known as the DNA binding/cleavage domain, and the third domain is the C-terminal tail, which is important for nuclear localization and contains amino acid sites that are important for phosphorylation and interactions with other proteins.^[3,18]

A major step forward in terms of structure-based drug design of novel DNA topoisomerase II α inhibitors was the de-

[a] B. Pogorelčnik, Dr. M. Brvar, Prof. T. Solmajer, Prof. A. Perdih
National Institute of Chemistry
Hajdrihova 19, 1001 Ljubljana (Slovenia)
E-mail: andrej.perdih@ki.si

[b] Prof. B. Žegura, Prof. M. Filipič
National Institute of Biology
Department of Genetic Toxicology and Cancer Biology
Večna pot 111, 1000 Ljubljana (Slovenia)

Supporting information for this article is available on the WWW under <http://dx.doi.org/10.1002/cmdc.201402459>.

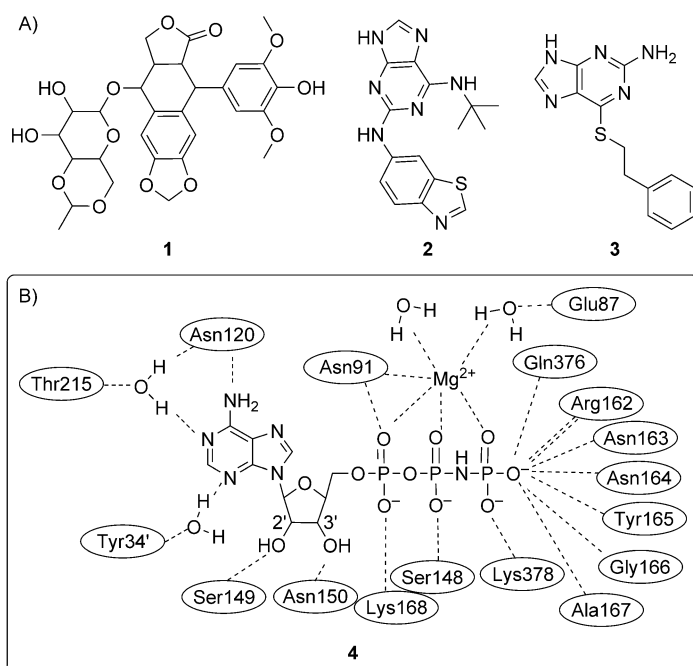


Figure 1. A) Structures of selected human DNA topoisomerase II α inhibitors: non-intercalative poison etoposide (**1**) and catalytic inhibitors **2** and **3**. B) Schematic *in silico* interactions between AMP-PNP (**4**) and a human ATPase domain as revealed by X-ray crystallography (PDB: 1ZXN).^[21] Dotted lines indicate hydrogen bonds.

termination of the crystal structure of the human ATPase domain in complex with a non-hydrolyzable ATP analogue (AMP-PNP (**4**)). As mentioned above, the ATPase domain is located on the N-terminal fragment of htlI α , and it has been broadly studied for potential inhibition.^[21] In Figure 1, crucial interactions are shown between AMP-PNP (**4**) and amino acid residues in the ATP binding pocket, as determined by X-ray crystallography. The crystal structure (PDB: 1ZXN) revealed that the adenine ring of the AMP-PNP molecule forms direct hydrogen bonds with Asn 120 and water-mediated interactions with Thr215 and Tyr34' (residue originating from another protomer of topo II α). Two hydroxy groups of the ribose form hydrogen bonds with the side chains of Ser 149 and Asn 150. The oxygen atoms in the three phosphate groups are involved in several interactions with residues from the ATP lid (see Figure 1B).^[21] Interestingly, Lys 378 from the QTK (Gln 376, Thr 377, Lys 378) loop^[22] of the transducer domain forms a salt bridge with the γ -phosphate. Finally, an Mg²⁺ ion is octahedrally orientated with all three phosphates, Asn 91, and two water molecules, whereas Glu 87 forms a water-mediated hydrogen bond with the Mg²⁺ ion. Residues Ile 125, Phe 142, Ile 141, Ile 217, and Asn 120 also contribute to nonpolar protein–ligand interactions.^[21]

Recently, several reports were published describing novel catalytic inhibitors that bind to the ATP binding site. For example: purine analogues (**2** and **3**),^[14, 23–26] different synthesized inhibitors from the imidazole, triazine class, thiosemicarbazone, and xanthone chemical classes,^[27–32] and natural products.^[33–36] Based on virtual screening and homology modeling experiments, researchers from Novartis^[14] developed a series of topo-

isomerase II α inhibitors (e.g., compound **2**) with a purine fragment that acts as a replacement for the adenine moiety in the AMP-PNP molecule. This model proposed that the purine scaffold forms direct hydrogen bonds with Asn 120 and Asn 91, whereas the propyl group was designed to fill the ribose sub-pocket of the ATP pocket by making favorable hydrophobic contacts with Ile 141, Phe 142, and Ala 167 residues.^[14] These hydrophobic residues were also observed in several other modeling studies.^[30, 37] Furthermore, a novel diphyllin glycoside with an acetylated D-quinovose sugar moiety and N-fused imidazoles possessing promising anti-topoisomerase activity were synthesized and characterized.^[27, 33]

In this study, we have focused our efforts on the identification of novel htlI α inhibitors by taking the available structural information about the binding of the AMP-PNP (**4**) molecule to topo II α as our starting point. The designed multistep workflow, where a plethora of *in silico* techniques were merged with experimental methods, is schematically depicted in Figure 2.

Results and Discussion

Design Phase I: structure-based virtual screening campaign from AMP-PNP–topo II α structure

A design starting point was provided by the structural information from the crystal structure of the htlI α ATPase domain co-crystallized with AMP-PNP (**4**) (PDB: 1ZXN).^[21] Using LigandScout pharmacophore software,^[39] we derived a structure-based pharmacophore model reflecting the interactions of the AMP-PNP molecule with the htlI α ATPase domain.^[21] The complete structure-based pharmacophore model of the AMP-PNP molecule in the ATP binding site generated by LigandScout^[39] is represented in the Supporting Information (Figure S1). To design small-molecule fragments that mimic the adenine moiety of the AMP-PNP molecule, this initial pharmacophore model was reduced. The reduced structure-based pharmacophore model depicted in Figure 3A describes crucial interactions of the AMP-PNP adenine moiety with the ATPase domain. The structure-based pharmacophore model comprised four pharmacophore features: one hydrogen bond donor modeling the interaction with Asn 120, two hydrogen acceptors: one describing the interaction with Thr215 via a conserved water molecule (W931), and another water-mediated (W933) hydrogen bond to Tyr 34' (from another protomer), and one hydrophobic feature. To find compounds with moieties that could act as replacements of the adenine moiety, two hydrogen bonds via conserved water molecules (W931 and W933) were also included.^[21] In comparison with other published models, a hydrophobic feature was added to the ribose moiety, due to the presence of several hydrophobic residues in its surroundings (e.g., Ile 141, Phe 142, and Ala 167).^[14, 30, 33, 37] This structure-based pharmacophore was used in a large-scale virtual screening campaign by LigandScout software using an in-house li-

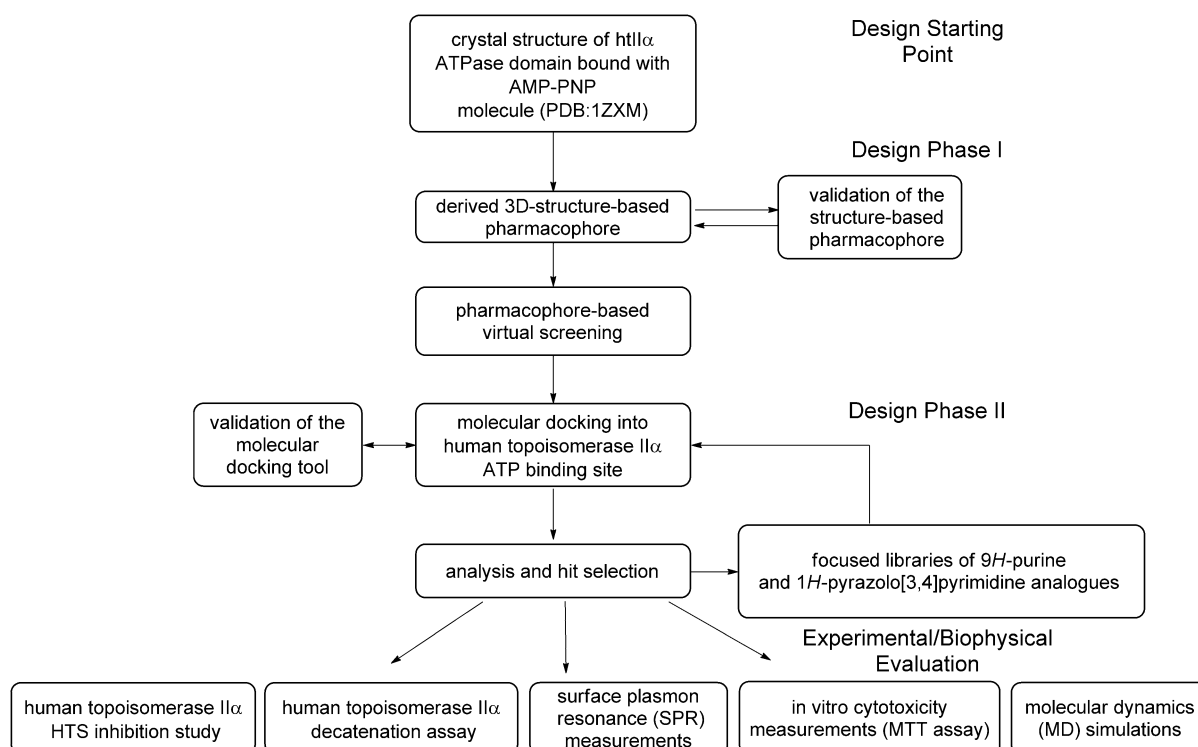


Figure 2. Schematic workflow^[38] used in the identification of novel human DNA topoisomerase II α inhibitors.

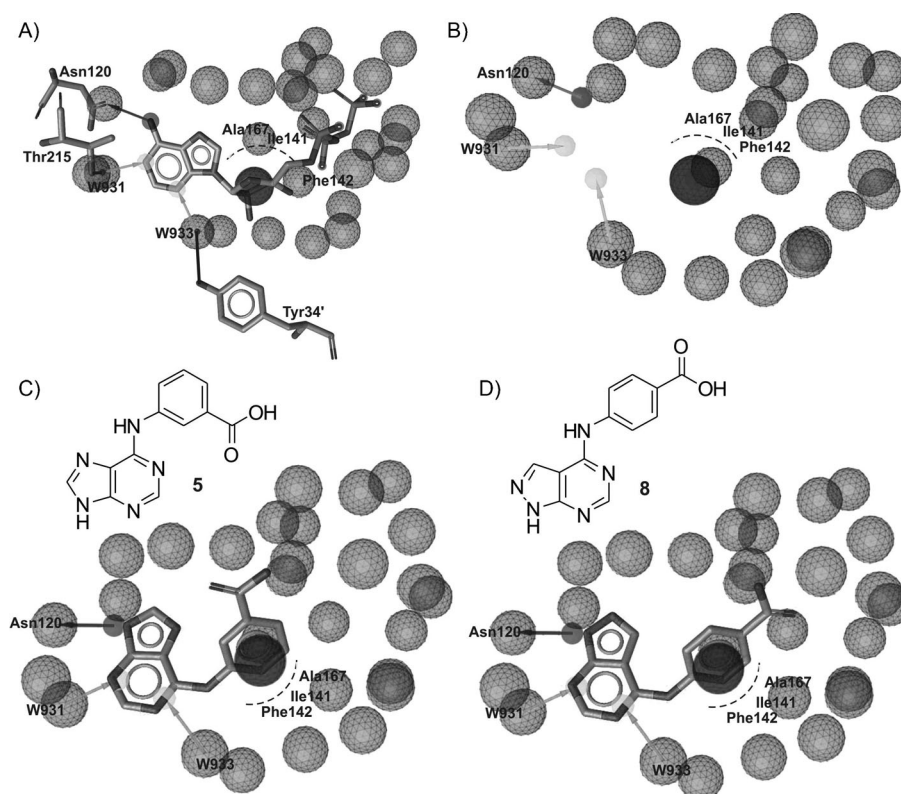


Figure 3. A) Derived reduced 3D structure-based pharmacophore model of the AMP-PNP molecule. B) 3D-structure-based pharmacophore model without amino acid residues used in our virtual screening campaign. C, D) Examples of virtual hits **5** and **8**, aligned with the pharmacophore model. Dark-grey arrows represent hydrogen bond donors, light-grey arrows show hydrogen bond acceptors, dark-grey spheres indicate hydrophobic interactions, and light-grey spheres show exclusion volumes.

library of six million commercially available compounds, which contained approximately 6200 adenosine-like structures^[40] (see Experimental Section for details concerning screening library preparation). Approximately 500 virtual hits from different chemical classes were obtained from the screening procedure. Examples of the novel hits identified by LigandScout^[39] include mono-substituted compounds of the established purine class (e.g., compound **5**), as well as compounds from the pyrazolopyrimidine class (compound **8**), which are presented in Figure 3C,D (see Figure S2 for LigandScout-generated alignments of selected inactive compounds from both classes). Overall, the chemical diversity of the identified hit compounds comprised several other scaffolds from different chemical classes (e.g., 1,2,4-triazol-1,5-pyrimidines and thiadiazoles).

Approximately 500 hits obtained in the first stage of the

virtual screening campaign were docked into the htl α ATPase domain using the GOLD molecular tool.^[41] A validation of the docking model was done by redocking the AMP-PNP molecule in the ATPase domain (see Figure S3). In the docking experiments, a pharmacophoric constraint (Asn120 as a hydrogen bond donor) was introduced to assure that this interaction with this important residue was always present.^[21] In addition, the conserved water molecules (W931 and W933) that were also shown to be important in hydrogen bond interactions experimentally^[21] were included in the docking calculations. Assessment of the docking poses was performed with the ChemScore scoring function, which showed the most optimal behavior relative to the experimental results (see description of validation in the Experimental Section). After the docking procedure, binding geometries, values of scoring function, values of pharmacophore fit scoring function, and hydrogen bond distances between heteroatoms of the docked ligands and amino acid residues were analyzed. Obtained binding geometries were first visually inspected and carefully analyzed for potential interactions with the amino acid residues that were hypothesized to be important for binding: a hydrogen bond with Asn120 and hydrophobic interactions with Ile141, Phe142, and Ala167.

Comparison of the docked AMP-PNP molecule and compounds from the 9*H*-purine (**5**) class and 1*H*-pyrazolo[3,4]pyrimidine (**8**) classes indicated that the 9*H*-purine ring of com-

pound **5** and the 1*H*-pyrazolo[3,4]pyrimidine ring of compound **8** overlapped with the adenine fragment of the AMP-PNP molecule, whereas the benzene moiety overlapped with the ribose moiety and one phosphate group of the AMP-PNP (see Figure S4 for details). As indicated in the docking model between compounds **5** and **8** and the ATPase domain, the 9*H*-purine and 1*H*-pyrazolo[3,4]pyrimidine rings formed direct hydrogen bonds with Asn120 and Thr215, whereas the benzene ring was anchored in the hydrophobic pocket surrounded by residues Ile141, Phe142, and Ala167. Finally, the carboxylic acid formed a hydrogen bonds with residues Ser149 and Asn150 (Figure 4A,B). In the case of compound **8** from the 1*H*-pyrazolo[3,4]pyrimidine class, the carboxylic acid group formed an additional hydrogen bond with Ser148. Compounds **5**–**11** from the aforementioned compound classes were selected for experimental evaluation (see Table S5 for compound origin details and vendor quality control procedures).

Biological activity of the selected compounds was determined using a standard htl α assay (see Experimental Section). The inhibitory htl α assay was first validated using reference compounds etoposide (**1**) and NSC35866 (**3**). The obtained IC₅₀ value of 33.8 μ M for **1** was in good accordance with the IC₅₀ value reported in the literature (60.3 μ M),^[42,43] as was the IC₅₀ value established for compound **3** (IC₅₀ = 85 μ M) compared with that reported earlier (IC₅₀ = 50 μ M).^[25] It was gratifying to observe that four compounds from the two structural classes

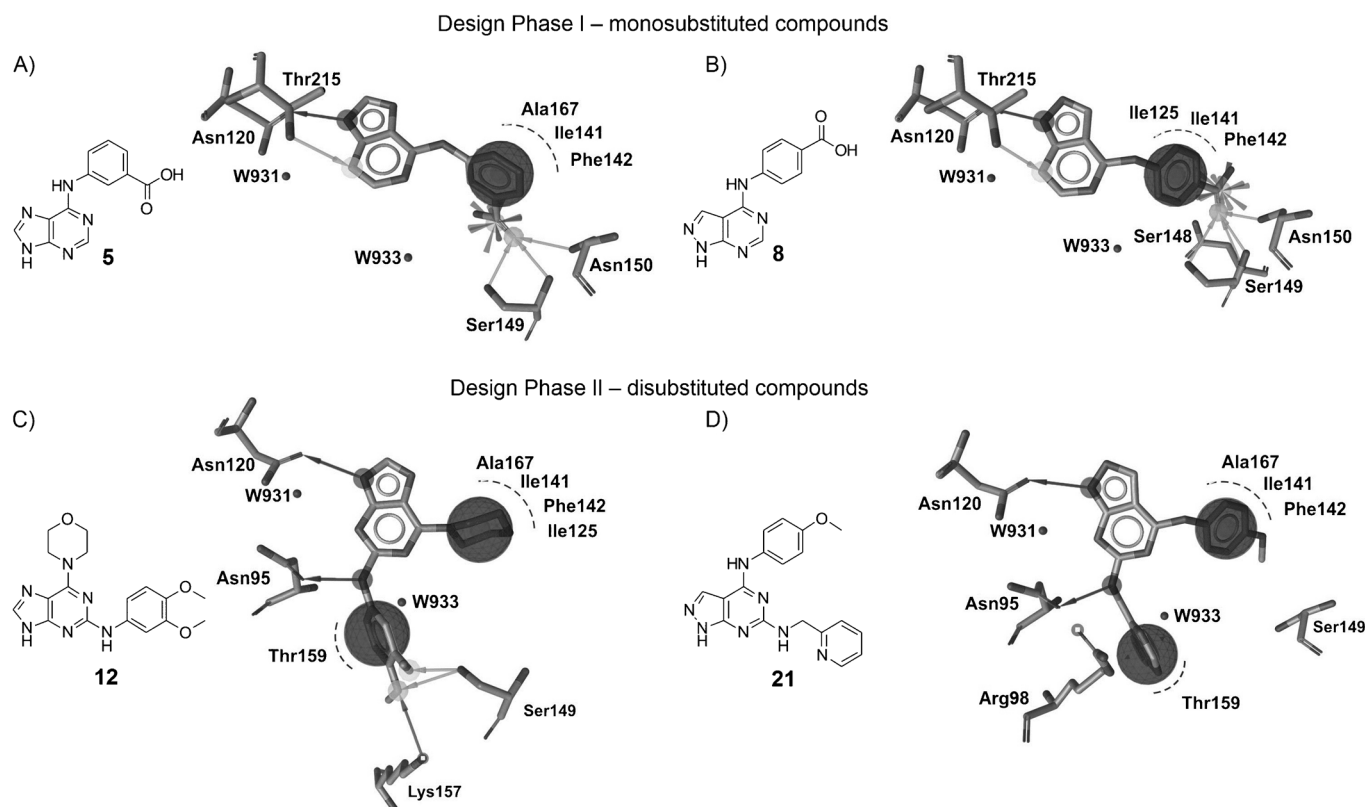


Figure 4. GOLD-calculated binding modes of mono- and disubstituted purine-based compounds **5** and **12** and pyrazolopyrimidine-based compounds **8** and **21** from design stages I and II. Residues important for binding are shown in grey, dark-grey arrows represent hydrogen bond donors, light-grey arrows show hydrogen bond acceptors, and hydrophobic interactions derived by LigandScout are depicted as dark-grey spheres. For clarity, exclusion volume spheres are not shown.

selected on the basis of the performed virtual screening campaign—namely, compounds **5** and **6** from the *9H*-purine class, and compounds **8** and **9** from the *1H*-pyrazolo[3,4]pyrimidine class—exhibited inhibitory activity against htl α in the lower micromolar range. Moreover, the compounds from the *1H*-pyrazolo[3,4]pyrimidine class represent, to the best of our knowledge, the first compounds containing this scaffold with the ability to inhibit this enzyme. The discovered *9H*-purine compounds displayed further novel possibilities offered by this scaffold for htl α inhibition. The obtained inhibitory values were similar to those of the established reference htl α inhibitors from the literature: etoposide (**1**) and NSC35866 (**3**). Detailed results of the inhibition assay are further presented in Figure S5. These active compounds were also tested against bacterial DNA gyrase in a standard inhibition assay,^[44] and results are presented in Table 1. To eliminate aggregation and

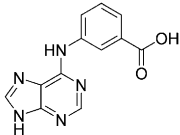
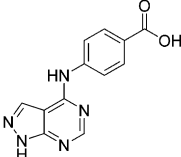
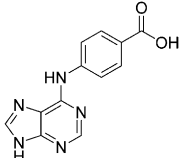
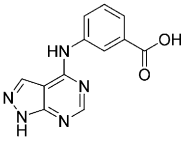
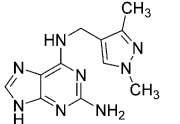
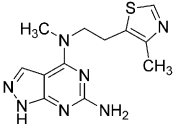
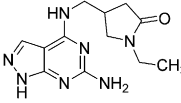
class contained a pyrazolopyrimidine fragment which, according to in our in silico model, could potentially serve as replacements of the adenine moiety interacting with Asn120. The second fragment is a benzene ring with *meta* or *para* position of the carboxylic group which according to our model can interact with hydrophobic residues located in the vicinity of the ribose moiety of the AMP-PNP molecule. Due to the presence of the carboxylic group in all active compounds, we immediately suspected that penetration through the cell membrane could pose a problem for these compounds, thus we decided to focus our design efforts on finding more lipophilic compounds. Obtained *clogP* values for the active compounds **5**, **6**, **8**, and **9** were found to be in the interval between 2.4–2.6 (see Table S5). To obtain effective and lipophilic inhibitors, focused libraries of approximately 200 analogues of *9H*-purine and *1H*-pyrazolo[3,4]pyrimidine were assembled from our in-house libraries of commercially available

compounds. Initial 3D structures were generated with OMEGA^[46] and docked into the human ATPase domain^[21] using GOLD software.^[41] Their calculated docking poses were visually inspected for potential interactions with amino acid residues of the binding site using LigandScout software.^[39] Unfortunately, compounds from both classes that would retain the benzene ring with the carboxylic group in a *meta* or *para* position were not available. Thus, we selected several alternatives at the R² position (e.g., morpholine analogues and *meta*- or *para*-substituted benzenes), also taking into account the structure–activity relationship results from previous *9H*-purine studies.^[14,23] In addition, during compound selection, we included new additional substitutions at the C2 position, which was left unsubstituted in design phase I. Previously, C6

substitution was also shown to be favorable.^[14] In summary, with these modifications, we wanted to increase the possibilities for compound activity at the cellular level while preserving and optimizing the interaction pattern. Eight disubstituted compounds from the *9H*-purine class (**12**–**19**) and ten disubstituted compounds from the *1H*-pyrazolo[3,4]pyrimidine class (**20**–**29**) were finally selected (see Table S5 for selected compound details and vendor quality control procedures) and assayed for their htl α inhibitory activity, with results presented in Tables 2 and 3 (see Figure S5 for further inhibitory assay data).

The obtained docking poses of the selected disubstituted compounds from both focused libraries showed similar interac-

Table 1. Inhibitory activities toward htl α and bacterial DNA gyrase determined for compounds **5**–**11** identified in design phase I.

| Compd | IC ₅₀ [μ M] ^[a] | | Compd | IC ₅₀ [μ M] ^[a] | |
|---|--|--------|---|--|--------|
| | htl α | gyrase | | htl α | gyrase |
|  | 65 ± 3.3 | > 1000 |  | 44 ± 5.8 | > 1000 |
|  | 142 ± 3.9 | > 1000 |  | 279 ± 14.4 | > 1000 |
|  | > 1000 | ND |  | > 1000 | ND |
| | | |  | > 1000 | ND |

[a] Data are the mean ± SD of *n* = 2 independent experiments performed in duplicate; ND: not determined.

nonspecific inhibition, a surfactant (Tween 20) was added to the reaction mixture.^[45] Selected *9H*-purine **7** and *1H*-pyrazolo[3,4]pyrimidines **10** and **11**, all containing a free NH₂ group without any additional fragments, which according to our model, could form an interaction with Ser149, did not show any inhibition activity.

Design Phase II: disubstituted *9H*-purine and *1H*-pyrazolo[3,4]pyrimidine compounds with improved lipophilicity

In the first step of our structure-based drug design efforts inhibitors, two different core fragments were successfully identified. One class of molecules contained purine, and the other

Table 2. Determined htl α inhibitory activities of disubstituted 9H-purine compounds **12–19**, selected in design phase II.

| Compd | R ¹ | R ² | IC ₅₀ [μ M] ^[a] |
|-----------|----------------|----------------|--|
| 12 | | | 145 \pm 2.8 |
| 13 | | | 211 \pm 12.7 |
| 14 | | | 258 \pm 14.9 |
| 15 | | | 462 \pm 38.0 |
| 16 | | | > 1000 |
| 17 | | | > 1000 |
| 18 | | | > 1000 |
| 19 | | | > 1000 |

[a] Data are the mean \pm SD of $n=2$ independent experiments performed in duplicate.

tion patterns to those observed previously (hydrogen bonds with Asn120 and Ser149 and hydrophobic interactions with the lipophilic pocket), along with an additional hydrogen bond with Asn95. In Figure 4C, one of the most active disubstituted compounds, *N*-(3,4-dimethoxyphenyl)-6-(morpholino)-9H-purin-2-amine (**12**), is shown to form a direct hydrogen bond with Asn120. An amine linkage at the R² position forms a hydrogen bond with Asn95, two methoxy groups form hydrogen bonds with Ser149, and one methoxy group forms a hydrogen bond with Lys157, whereas the R² morpholine group is positioned in the hydrophobic pocket filled with residues Ile141, Phe142, and Ala167. These observations are in line with molecular modeling observations of a series of purine analogues in the ATPase domain reported previously.^[14] Introduction of 1,2-dimethoxybenzene (**12** and **13**) or a methoxybenzene moiety (**14**) at R² resulted in a moderate inhibitory activity against htl α (IC₅₀=145 μ M, 211 μ M, and 258 μ M, respectively). The absence of these moieties resulted in a loss in inhibitory activity (compounds **16–19**). Interestingly, an additional methoxy group attached on the benzene fragment at the R¹ position of compound **13** did not increase the inhibitory activity. On the other hand, compound **15**, with a fluorophenyl moiety at R², showed weak activity (IC₅₀=462 μ M). Further analysis of the binding poses compounds **16–19** that were inactive showed an absence of the interaction with Ser149 (see Figure S6A). Obtained clogP values for active compounds **12–14** were found to be in the interval between 2.4 and 4.6 (see Table S5).

A similar interaction pattern was found for the docked active compounds **20** (IC₅₀=57 μ M) and **21** (IC₅₀=67 μ M)

Table 3. Inhibitory activities against htl α for disubstituted 1H-pyrazolo[3,4]pyrimidine compounds **20–29** selected in design phase II.

| Compd | R ¹ | R ² | IC ₅₀ [μ M] ^[a] |
|-----------|----------------|----------------|--|
| 20 | | | 57 \pm 4.1 |
| 21 | | | 67 \pm 2.8 |
| 22 | | | 360 \pm 23.3 |
| 23 | | | 449 \pm 38.9 |
| 24 | | | 508 \pm 34.8 |
| 25 | | | 578 \pm 29.8 |
| 26 | | | > 1000 |
| 27 | | | > 1000 |
| 28 | | | > 1000 |
| 29 | | | > 1000 |

[a] Data are the mean \pm SD of $n=2$ independent experiments performed in duplicate.

among the disubstituted pyrazolopyrimidines. In both compounds, the amine group of the pyrazolopyrimidine ring forms a hydrogen bond with Asn120, the amine group at R² forms a new hydrogen donor bond with Asn95, and the methoxy phenyl is capable of forming hydrophobic interactions with the hydrophobic pocket containing residues Ile141, Phe142, and Ala167. Moreover, the pyridine ring R² substitution also forms π - π interactions with Arg98 (Figure 4D), as in the case of compound **21**.

Pyrazolopyrimidine-containing compounds **26–29** were found to be inactive (IC₅₀>1000 μ M). Inspection of the GOLD-calculated binding mode revealed the lack of interaction with Asn95 in compounds **26–29**. Proposed GOLD binding mode for selective inactive compound **29** is available in Figure S6B. The absence of hydrogen in the piperazine fragment at the R² position resulted in a significant decrease in activity of compounds **26** and **29** when tested in the inhibitory assay compared with the amine linkage in active compounds. Obtained clogP values for the most active compounds, **20–22**, were found to be favorable (Table S5). Overall, our optimization efforts in design phase II did not result in significant improvement of the htl α inhibitory properties, and compounds that came out of both design phases are still inferior relative to some of the similar reported catalytic inhibitors.^[6] Nevertheless, we were able to identify several interesting compounds of the newly discovered 1H-pyrazolo[3,4]pyrimidine class and estab-

lished compounds from the 9H-purine class with promising htl α inhibitory activities, and in the second stage, we identified compounds with favorable characteristics for potential cellular activity.

Human DNA topoisomerase II α decatenation assay

To explore whether the compounds from both classes (**8** and **12**) could also inhibit catalytic activity of the htl α enzyme, the effect of compounds on the enzyme catalytic activity was evaluated using a kDNA decatenation assay. The decatenation assay was performed in duplicate, as described in the Experimental Section, with selected compounds using kinetoplast (kDNA) as a substrate and etoposide (**1**) as a reference compound. The results of the kDNA decatenation assay for compounds **8** and **12** are presented in Figure 5.

As shown in Figure 5, compounds **8** and **12** significantly inhibited the decatenation of kDNA in a concentration-dependent manner (see also Table S2). Almost no decatenation activity was observed in the presence of 500 and 125 μM of compound **12** or in the presence of 500 μM for compound **8**. Moderate activity was observed at 31.5 μM of compound **12**. Overall, these results confirmed the influence of both compounds on the catalytic activity of htl α , with compound **12** exhibiting similar to slightly improved inhibitory activity against htl α decatenation as the inhibitor etoposide (**1**).

Biophysical characterization and MD simulations of the 1H-purine and 1H-pyrazolo[3,4]pyrimidine htl α inhibitor classes

SPR measurements

We subsequently investigated if the inhibitory activity of compounds **8** and **12** was associated with their binding to the

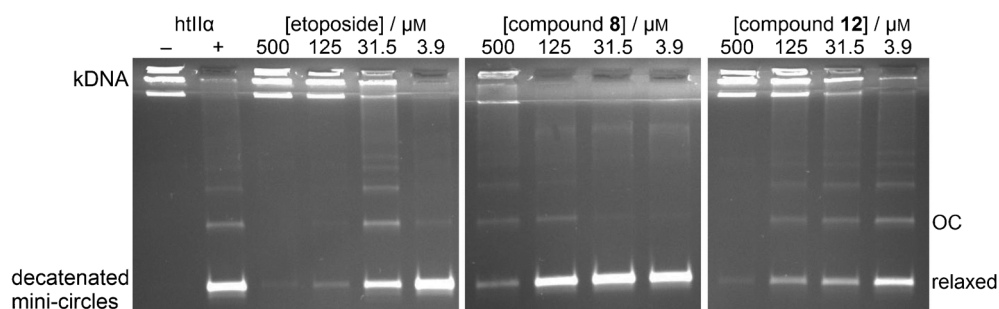


Figure 5. Compounds **8** and **12** inhibited DNA decatenation catalyzed by htl α . Each reaction contained the same amount of htl α and solvent DMSO (1%), except in the case of the negative control reaction of kDNA, which was performed in the absence of htl α . The positive control band is indicated by (+). Etoposide (**1**) was used as a reference compound. The positions of bands, including open-circular DNA (OC), are also indicated.

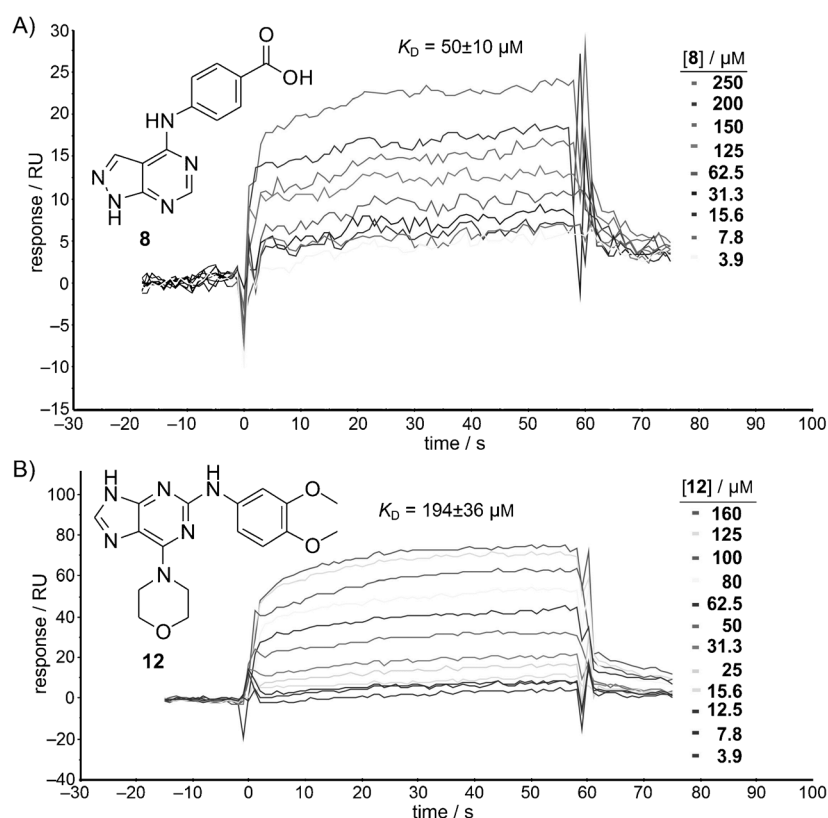


Figure 6. SPR studies of the 9H-purine and 1H-pyrazolo[3,4]pyrimidine classes of htl α inhibitors, with representative sensorgrams for compounds A) **8** and B) **12**. The binding experiments were performed on a BiacoreX at a flow rate of 30 $\mu\text{L min}^{-1}$ at 25 °C in running buffer (10 mM HEPES pH 7.4, 150 mM NaCl, 3 mM EDTA, 0.005 % surfactant P20).

htl α ATPase domain using surface plasmon resonance (SPR) experiments (Figure 6).^[47,48] The ATPase domain of htl α was immobilized on the CM5 chip, and its activity was confirmed using etoposide (**1**) as a reference. Real-time sensorgrams were recorded and analyzed using BIAeval 3.1 software (Biacore, GE Healthcare) and are provided in Figure S7. General fitting and steady-state affinity (one-site binding) were calculated using Origin 6.1 (measured K_D value of $30 \pm 2 \mu\text{M}$ for etoposide in comparison with 41.6 μM , as reported in reference [35]). After validation of the SPR method, 1H-pyrazolo[3,4]pyrimidine com-

pound **8** was tested at nine different concentrations and 1*H*-purine compound **12** at 12 concentrations, both in at least three parallel experiments, and the K_D values were determined using a steady-state affinity binding model (one-site binding). The maximal theoretical response was calculated according to the molecular masses of the human ATPase domain and ligands **8** and **12**. These results confirmed binding of compounds **8** and **12** to the htl α ATPase domain and, consequently, formation of the ligand–enzyme complex. We were pleased to establish that K_D values for both compounds **8** and **12** were in good agreement with the determined IC_{50} inhibitory activity values (Table 4). Steady-state affinity analysis disclosed a K_D value of $50 \pm 10 \mu\text{M}$ for compound **8** and a K_D value of $194 \pm 36 \mu\text{M}$ for compound **12**. These SPR experiments consequently provided more confidence in our *in silico* models of binding generated by molecular docking studies of both compound classes. In addition, these experiments confirmed that both compounds bind to the human ATPase domain, and they do not form a covalent cleavable complex. It should be noted that, recently, a powerful flow linear dichroism (FLD) technique for continuous monitoring of the topoisomerization reaction was reported, enabling in-depth mechanistic studies of topo enzymes and their interactions with ligands.^[49] This promising new approach could complement the SPR studies, offering further insight into the inhibition process of our discovered compounds.

MD simulations of the proposed complexes of compounds **8** and **12** with the htl α ATPase domain

To provide further insight into the dynamic behavior of the compounds from the 9*H*-purine and 1*H*-pyrazolo[3,4]pyrimidine classes of htl α inhibitors, MD simulations^[50] were initiated for the docked conformation of inhibitors **8** (1*H*-pyrazolo[3,4]pyrimidine) and **12** (9*H*-purine) in the htl α ATP active site using CHARMM software.^[51] Experimental data supporting the use of the initial binding mode was substantiated by our SPR data, confirming the binding of this

Table 4. Comparison of the obtained IC_{50} and K_D values for compounds **8** and **12**.^[a]

| Compd | IC_{50} [μM] | K_D [μM] |
|-----------|-----------------------------|-------------------------|
| 8 | 44 ± 5.8 | 50 ± 10 |
| 12 | 145 ± 2.8 | 194 ± 36 |

[a] IC_{50} values are from two independent experiments; K_D values are the mean \pm SD of $n=3$ independent experiments performed in triplicate.

compound to the htl α ATPase domain. Constructed solvated protein–ligand (**8** and **12**) systems were prepared, equilibrated, and simulated as described in Supporting Information Section 4.3 and are presented schematically in Figure 7 A. Anima-

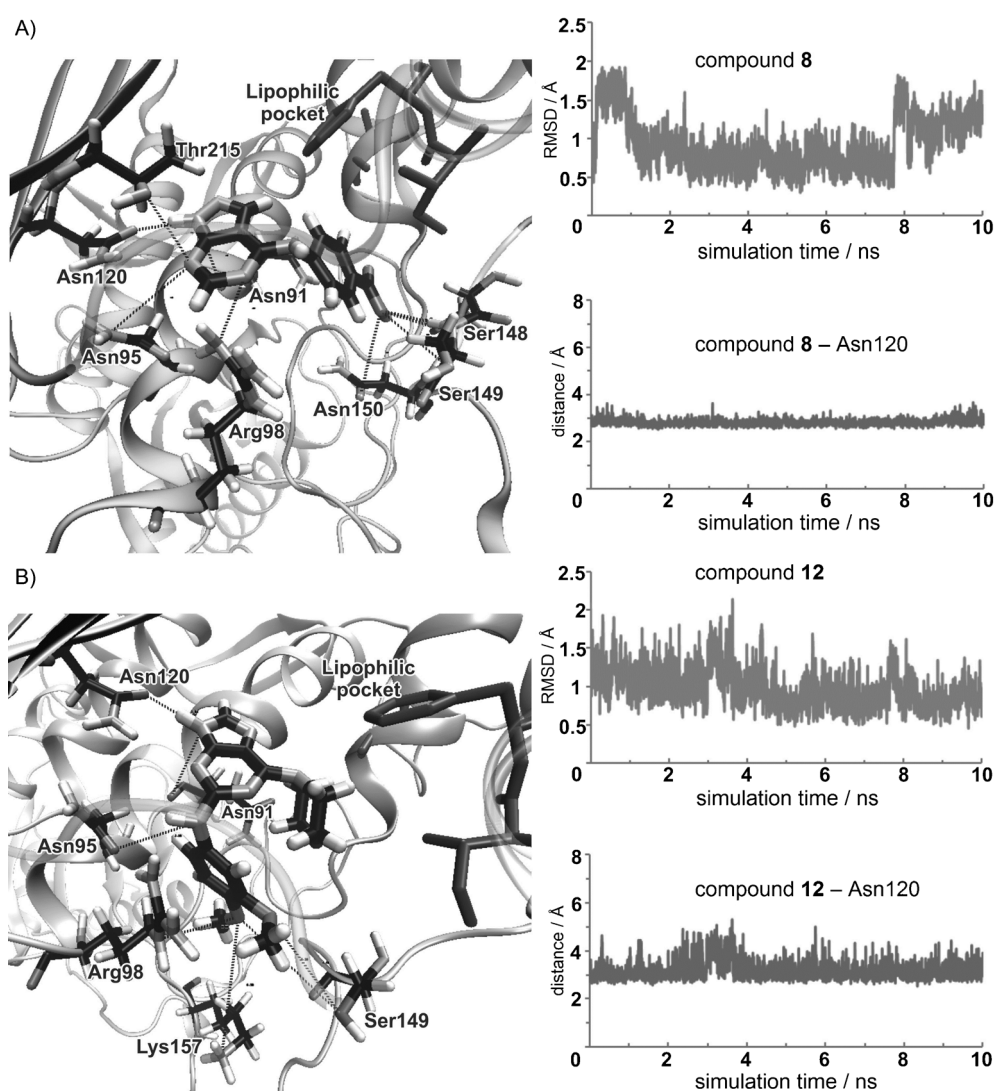


Figure 7. MD simulation studies of the 9*H*-purine and 1*H*-pyrazolo[3,4]pyrimidine classes of htl α inhibitors. A) Left: MD snapshot of 1*H*-pyrazolo[3,4]pyrimidine-based compound **8** in the solvated ATP binding site of the htl α protein; Right: time dependence of RMSD, and distance between the OD1 oxygen atom of Asn120 and the N4 nitrogen atom of the pyrazole fragment in compound **8**. B) Left: MD snapshot of 9*H*-purine-based compound **12** docked into the solvated ATP binding site of the htl α protein; Right: time dependence of RMSD and distance between the OD1 oxygen atom of Asn120 and the N3 nitrogen atom of the purine ring in compound **12**.

tions of the calculated production phase with 10 ns MD trajectories for both compounds are available in the Supporting Information.

The production 10 ns MD trajectories were first analyzed to determine the stability of the ligand pose in the topo II α ATP binding site. RMSD (root mean square distance) time-dependent graphs (Figure 7B) shows deviation between the MD-generated conformations and the docking conformations, calculated with all atoms taken into consideration. The obtained RMSD averages of 0.93 ± 0.34 Å (compound **8**) and 0.98 ± 0.26 Å (compound **12**), calculated from the average structure, indicated relatively stable binding conformations (Figure 7).

Next, we analyzed several docking-proposed hydrogen bond distances (see Supporting Information Section 2.2 and Figure 4) between investigated compounds **8** and **12** and residues in the htlI α ATP binding site.^[21] The hydrogen bond interactions were monitored between atoms of compound **8** and corresponding GOLD-proposed interacting residues Asn120, Ser148, Ser149, Asn150, and Thr215. For compound **12**, proposed interactions between Asn95, Asn120, Ser149, and Lys157 were investigated (see Figure 4 for docking modes of **8** and **12**). In addition, after visualization of the MD trajectories, the following residues were also analyzed (compound **8**: Asn91, Asn95, Asn98; compound **12**: Asn91, Arg98, Asn150, Thr215). Time-dependence graphs of all monitored distances are available in the Supporting Information (see Figure S9A–S) and selected time-dependence graphs of interactions of Asn120 with **8** and **12** are presented in Figure 7. Values of calculated average distances are available in Table 5.

In both cases, the carbonyl oxygen of Asn120 formed a stable hydrogen bond acceptor interaction with the corresponding nitrogen of the heterocyclic moieties of compounds **8** and **12**. The observed average distance of 2.82 ± 0.14 Å for

compound **8** correlates nicely with the higher determined K_D and IC_{50} values with respect the 3.17 ± 0.43 Å value observed for compound **12** (Figure 7). These results are in accordance with the proposed interaction pattern observed in the docking calculations for the studied heterocyclic moieties that are core to both classes. The predicted hydrogen bond acceptor interaction between Thr215 and the pyrazolo[3,4]pyrimidine core of compound **8** was shown to be weak (3.92 ± 0.28 Å). Next, Asn95 which was also suggested as a potential interacting residue for 9H-purine compound **12** showed a hydrogen bond interaction in the 3.54 ± 0.62 Å range. When visualizing the MD trajectories, additional moderate interactions were observed with the Asn91 and Arg98 residues for both compounds.

Interestingly, moieties attached to the 9H-purine and 1H-pyrazolo[3,4]pyrimidine cores did not show the stable hydrogen bond interactions observed in the docking poses with amino acid residues Ser148, Ser149, Asn150, and Lys157 (Table 5). These observations could be rationalized by a slightly increased level of conformational flexibility of the attached 4-carboxyl-phenyl moiety in the case of the 1H-pyrazolo[3,4]pyrimidine molecule, whereas in the case of purine compound **12**, the observed movement of the protein loop located between residues 145 and 165 could provide some initial clues. In the ATP binding site, the lipophilic area encompassed by amino acids Ile141, Phe142, and Ala167 was found to favorably interact with benzene (**8**) and morpholine (**12**) moieties. Another interesting observation occurred when we visualized the water molecules surrounding the ATP binding site and ligand molecules. Over the course of the MD simulation, the number of water molecules surrounding compounds **8** and **12** in the ATP binding site increased. Overall, the results of the MD simulations provided initial dynamic insight into the conformational behavior of ligands **8** and **12**. The most important interaction seemed to form between Asn120 and the 9H-purine and 1H-pyrazolo[3,4]pyrimidine core fragments.

Table 5. Calculated average interaction distances between compounds **8** and **12** and selected htlI α residues in the ATP binding site from MD simulation studies.

| Interacting Residues | Distance [Å] ^[a] | |
|--------------------------|-----------------------------|-----------------|
| | Compd 8 | Compd 12 |
| Asn91-O ^[b] | 3.82 ± 0.30 | 4.06 ± 0.34 |
| Asn95-ND2 | 3.92 ± 0.28 | ND |
| Asn95-OD1 | ND | 3.54 ± 0.62 |
| Arg98-NE ^[b] | ND | 4.17 ± 0.40 |
| Arg98-NH1 ^[b] | 4.05 ± 0.42 | ND |
| Asn120-ND2 | 3.31 ± 0.23 | 4.34 ± 0.39 |
| Asn120-OD1 | 2.82 ± 0.14 | 3.17 ± 0.43 |
| Ser148-OG | 4.22 ± 1.31 | ND |
| Ser149-N | 4.52 ± 1.39 | ND |
| Ser149-OG | 5.53 ± 1.44 | 4.29 ± 0.94 |
| Ser149-OG | 6.76 ± 1.18 | 6.05 ± 1.49 |
| Asn150-OD1 | 5.72 ± 1.37 | 4.59 ± 0.70 |
| Asn150-ND2 | 3.99 ± 1.18 | 4.09 ± 0.70 |
| Lys157-NZ | ND | 5.70 ± 1.41 |
| Thr215-OG1 | 3.97 ± 0.32 | 4.66 ± 0.44 |

[a] Average values and corresponding SD were calculated from 5000 equidistant conformations sampled from 10 ns MD simulations; ND: not determined. [b] Residues in italics were subsequently included in the analysis.

MTT cytotoxicity assays of the 9H-purine and 1H-pyrazolo[3,4]pyrimidine htlI α inhibitor classes

We evaluated active compounds **5**, **6**, **8**, **9**, **12–14**, and **20–22** for their in vitro cytotoxicity against two human cancer cell lines: MCF-7 (breast cancer), and HepG2 (hepatoma), while HUVEC cells (human umbilical vein endothelial cells) were used as non-cancer cells. Both selected human cancer cell lines, MCF-7 and HepG2, are representative and well-established systems for cell-based evaluation of potential anticancer compounds, and the HUVEC cell line provided critical comparison of non-cancer cell growth inhibition. The decrease in cell viability was determined by the tetrazolium-based colorimetric assay (MTT assay) and compared with the decrease in cell viability by etoposide at a concentration of $40 \mu\text{M}$, which was used as the positive control. In the first step, the exponentially growing cells were exposed to the compounds at a single concentration ($200 \mu\text{M}$) for 24 h. Compounds **13** (9H-purine) and **22** (1H-pyrazolo[3,4]pyrimidine) from the second stage significantly decreased the viability of cell lines at one concentration ($200 \mu\text{M}$). For the two most effective compounds, **13** and **22**,

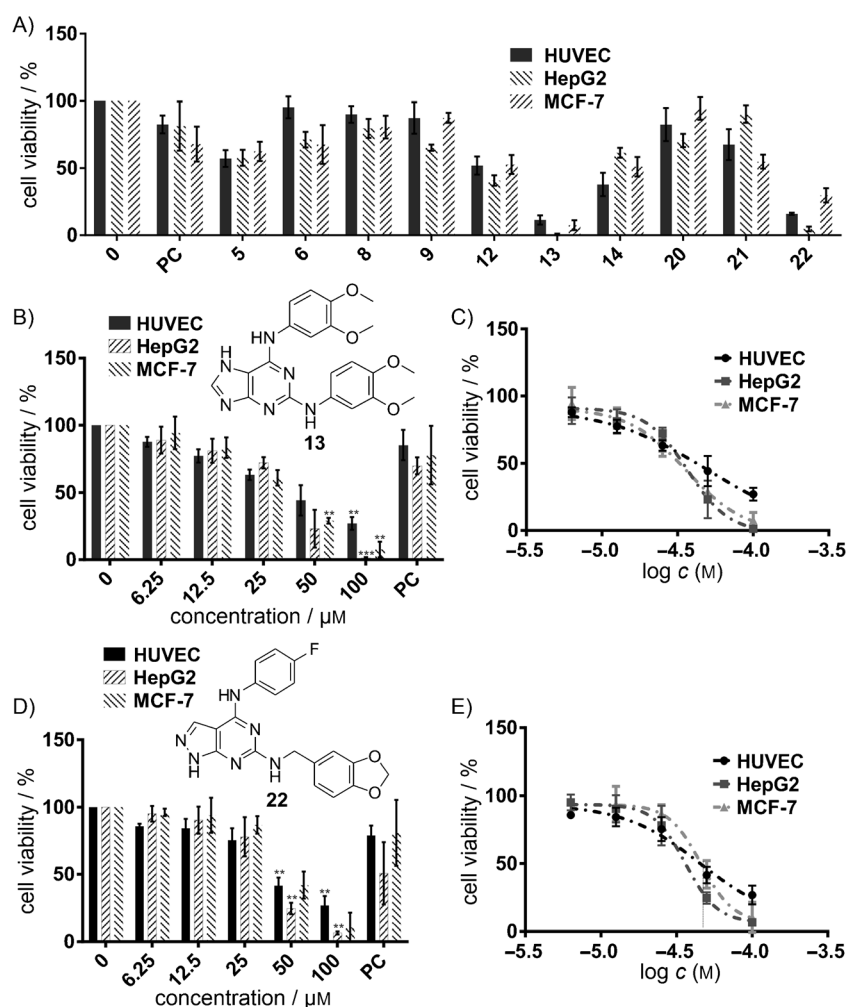


Figure 8. Results of the MTT cell viability assay. A) HUVEC, HepG2, and MCF-7 cells were treated with active compounds **5**, **6**, **8**, **9**, **12–14**, and **20–22** at 200 μM for 24 h. Etoposide (**1**) at 40 μM was used as positive control (PC), and DMSO (1%) was used as vehicle control. The data are presented as percent cell viability relative to vehicle-treated cells (data not shown). B,D) HUVEC, HepG2, and MCF-7 cells were exposed to various concentrations (100, 25, 12.5, and 6.25 μM) of compounds **13** and **22**. C,E) Dose-response curves of log concentration versus percent viability of cells for compounds **13** and **22**. Data represent the mean \pm SD of three experiments; significant differences between the vehicle control and treated cells: ** $p < 0.01$, *** $p < 0.001$.

which reduced cell viability by more than 80% relative to the untreated control, EC_{50} values were determined by testing their cytotoxicity at concentrations ranging from 6.25 to 100 μM (Figure 8B, D). Figure 8C, E shows that both compounds caused a dose-dependent decrease in the viability of all three types of cells.

At a concentration of 100 μM , compound **13** significantly decreased the viability of HUVEC, HepG2, and MCF-7 cells, whereas compound **22** significantly decreased the viability of HUVEC and HepG2 cells relative to the control (Figure 8B, D). At a concentration of 50 μM , compound **13** significantly decreased the viability of MCF-7 cells compared with the vehicle control, while compound **22** induced a significant decrease in the viability of HUVEC and HepG2 cells. At lower concentrations (6.25, 12.5, 25 μM), the two compounds did not significantly affect the viability of the three cell lines compared with the control.

From the EC_{50} values (Table 6), it is evident that compound **13** showed higher toxicity against HepG2 ($\text{EC}_{50} = 37.0$ μM) and

MCF-7 ($\text{EC}_{50} = 36.2$ μM) cancer cells than against the non-cancer HUVEC cells ($\text{EC}_{50} = 50.9$ μM). Compound **22** showed similar cytotoxicity against HepG2 ($\text{EC}_{50} = 36.2$ μM), HUVEC ($\text{EC}_{50} = 45.4$ μM), and MCF-7 ($\text{EC}_{50} = 45.9$ μM) cells. The inhibitory activity of compounds **13** and **22** against two cancer-derived cell lines (HepG2 and MCF-7) relative to the non-cancer-derived HUVEC cells was not statistically significant. The cytotoxicity of compounds **13** and **22** against cancer cells appear to be related to htl α inhibitory activity (Table 6). Compound **13**, with a lower IC_{50} value, was more effective against cancer cells than compound **22**. Nevertheless, a caveat must be stated that the higher cell-based activity of compounds **13** and **22** compared with the in vitro htl α inhibitory activity indicates a possibility that cell-based activity might not be related exclusively to this enzyme. As these compounds target the htl α ATP binding site, several protein kinases could also be affected by these compounds. Influences of structurally related 9H-purine compound **3** on both htl α and cyclin-dependent kinases (CDK) have been reported, with further suggestions that such dual inhibitors of htl α and CDK activity

may be useful as anticancer agents.^[25]

Compounds **5**, **6**, **8**, and **9**, which showed some of the strongest htl α inhibitory activity, all have a carboxylic group in their structure, which is a plausible reason for the displayed lower cytotoxic activity in the MTT assay. As mentioned before, this concern also stimulated us to develop a second stage of our virtual screening campaign. To investigate this further, we calculated clog P values for all compounds (available in the Sup-

Table 6. Determined cytotoxicities in HUVEC, HepG2, and MCF-7 cells for compounds **13** and **22**.

| Compd | EC_{50} [μM] ^[a] | | |
|-----------|---|------------------|------------------|
| | HUVEC | HepG2 | MCF-7 |
| 13 | 50.9 (38.5–67.3) | 37.0 (31.7–43.2) | 36.2 (29.8–43.9) |
| 22 | 45.5 (36.2–57.0) | 36.2 (31.4–41.8) | 45.9 (40.5–51.9) |

[a] Independent experiments were performed in five replicates and were repeated three times; values in parentheses are means (95%).

porting Information). The $\text{clog}P$ values for compounds **5** and **6** were found to be 2.4, and the $\text{clog}P$ value for **8** and **9** were 2.5. In both cases, each pair of compounds represents the corresponding positional isomers (Table 1). On the other hand, active compound **22** has a $\text{clog}P$ value of 5.2, and **13** has a $\text{clog}P$ value of 4.6, indicating better characteristics for successful penetration through the cell membrane. This observation could be one of the reasons for the higher cytotoxicity of compounds **13** and **22** over compounds **5**, **6**, **8**, and **9**. It is important to note that these active compounds also display some promising characteristics for further hit-to-lead optimization. For example, the topological surface area (TPSA) for active compounds **8**, **12**, **13**, and **22** was found to be lower than 120 (TPSA(**8**) = 98.44, TPSA(**12**) = 92.07, TPSA(**13**) = 110.09, and TPSA(**22**) = 91.63).^[52]

Conclusions

Httl α is an important target for the development of anticancer agents. In this study, a two-stage virtual screening campaign was used to yield novel compounds from the established 9H-purine class and a novel structural class of 1H-pyrazolo[3,4]pyrimidine compounds as httl α inhibitors with micromolar inhibitory activity. Our design starting point represented an experimentally determined structure of the complex between AMP-PNP and the httl α ATPase domain. In the first design stage, a structure-based pharmacophore model for the description of crucial interactions was constructed, and after the virtual screening campaign, combining pharmacophore models with molecular docking calculations, active monosubstituted compounds from the 9H-purine and 1H-pyrazolo[3,4]pyrimidines classes were found to be micromolar inhibitors in the in vitro inhibition assays. The compounds from the 1H-pyrazolo[3,4]pyrimidine class represent, to the best of our knowledge, the first compounds containing this scaffold that can inhibit this enzyme. Several active compounds were also tested in vitro against bacterial DNA gyrase and were found to be httl α -selective inhibitors. In the second design stage, computational investigations of the focused libraries of 9H-purine and 1H-pyrazolo[3,4]pyrimidine compounds, followed by inhibition assays, successfully provided novel disubstituted compounds from both series possessing improved properties in terms of cytotoxic activity against cancer cell lines. Two representative active compounds, **8** and **12**, one from each class, were found to inhibit httl α -mediated DNA decatenation. Binding characteristics of both discovered classes were characterized using SPR measurements, which confirmed binding of these compounds to the human ATPase domain and, consequently, the formation of the ligand–enzyme complex. Both proposed complexes between compounds **8** and **12** and httl α remained stable during the performed 10 ns MD simulation studies, and subsequent analysis provided dynamic insight into the observed interactions, highlighting Asn 120 as a crucial interacting residue. Disubstituted compounds **13** and **22** from the second design stage showed promising cytotoxic activity in HepG2 and MCF-7 cancer cell lines, and derivative **13** appears as the most promising compound with regard to potential anticancer activ-

ity. The cytotoxicity of compounds **13** and **22** showed a direct relationship with httl α inhibitory activity. These compounds displayed good characteristics for further hit-to-lead development. We believe that these novel reported compounds will help to pave the way to novel anticancer agents necessary to efficiently combat various cancers.

Experimental Section

Structure-based pharmacophore modeling and pharmacophore-based virtual screening

The crystal structure of the complex between the httl α ATPase domain and a non-hydrolyzable ATP (AMP-PNP) molecule (**4**) was retrieved from the Protein Data Bank (PDB: 1ZXN). A structure-based pharmacophore was derived for the bound conformation of compound **4** using LigandScout software, and the initial number of pharmacophoric interactions were reduced^[21] (see Figure S1). The resulting structure-based pharmacophore model used in the first stage of our design consisted of two hydrogen bond acceptors, one hydrogen bond donor, and a hydrophobic interaction sphere. Exclusion volumes were automatically added to model the steric circumference of the active site of httl α . The structure-based pharmacophore model was screened against approximately 6 million commercially available compounds present in our library using the LigandScout screening module.^[40] Our library was composed of compounds originating from several commercial vendors (e.g., Enamine, InterBioScreen, Vitas-M, ChemBridge, ChemDiv, LifeChemicals, etc.), with each compound converted into a multifunctional format (25 conformers for each compound in the library) using the idbgen module available in LigandScout, coupled with the OMEGA software.^[46] The default high-throughput settings were used for library generation: maximum number of output conformers per molecule = 25, RMS threshold to duplicate conformers = 0.8 Å, maximum number of all generated conformers per molecule = 30000, and maximum number of intermediate conformers per molecule = 4000.^[53] The Pharmacophore Fit scoring function was used to score hit molecules against the obtained structure-based pharmacophore model. The LigandScout screening procedure retrieved approximately 500 hit compounds, which were visually inspected to select different compound classes.

Molecular docking calculations

Molecular docking experiments were carried out using the GOLD docking tool.^[41] First, the GOLD docking tool was validated.^[54] AMP-PNP (**4**) was extracted from its binding site (PDB: 1ZXN) and redocked using the GOLD molecular docking tool.^[41] In the validation procedure, AMP-PNP was docked 10 times into the httl α ATPase domain by applying different parameters of the GOLD genetic algorithm (GA): population size = 100, selection pressure = 1.1, number of operations = 100000, number of islands = 5, niche size = 2, migrate = 10, mutate = 95, crossover = 95. Several different scoring functions (ChemScore, GoldScore and ChemPLP) and spin states of the water molecules W931 and W933 were used. The active site was defined as a 10 Å radius around reference ligand AMP-PNP, and hydrogen atoms were added to the protein. Mg²⁺ and all waters were removed, except W931 and W933, which were included due to their importance in molecular recognition. These waters were included in docking calculations, because it was previously assumed that they play an important role in the binding of the AMP-PNP molecule.^[21] To ensure that interactions similar to the

interaction pattern of the purine moiety in the AMP-PNP molecule would be obtained, a pharmacophore constraint was added to Asn 120,^[21] and a ChemScore scoring function was used. The binding pose of docked AMP-PNP resembled the experimentally determined conformation, which indicated that variables for docking were reliable (see Figure S3). The RMSD comparison of the docked conformations with experimental values were calculated. The best agreement between the crystallized and docked poses was obtained using the ChemScore function (RMSD = 0.9 Å). This scoring function and the docking settings described above were further used for molecular docking calculations of the selected hit compounds from the first and the second stage of our virtual screening procedure.

MD simulations of the complex between compounds 8 and 12 and the htlI α ATPase domain

Molecular dynamics (MD) calculations for the ATPase domain (PDB: 1ZXM) with the corresponding docked conformation of compounds 8 and 12 were performed using the CHARMM molecular modeling suite.^[51] The bound conformations in the ATP binding site were generated as described in the Experimental Section (*Molecular docking calculations*) using the GOLD molecular docking suite. In the PDB file (1ZXM), missing side chain atoms were reported for the residues Lys 101, Lys 123, Lys 176, Asn 210, Glu 212, Lys 265, Lys 278, Lys 287, Val 288, Met 303, Lys 343, and Lys 400. In addition, protein loop residues between 345 and 350 were not observed in the experimental electron density map. All of these residues are mostly located on the protein surface and do not form direct interactions with the ATP binding site and the investigated compounds. The missing side chain atoms of these residues, as well as missing loop residues, were generated using the PDB Hydro web server (lorentz.immstr.pasteur.fr/pdb_hydro.php [accessed September 2014]) in a two-stage procedure.^[55] In the first stage, the 1ZXM crystal structure was submitted to the PDB Hydro web server to construct the missing protein loop. The PDB Hydro web server detected automatically the missing loop residues from the numbering and built them into the 1ZXM structure using an algorithm based on Monte Carlo moves.^[56] Subsequently, the resulting structure with the generated loop was retrieved and visually inspected to assess the produced loop conformation. In the second stage, this structure was submitted to another available module on the PDB Hydro server where missing side chains were detected, and possible rotamers of these side chains were scanned selecting the conformation with the lowest van der Waals (vdW) energy. This procedure was performed sequentially for each residue to yield the final structure with all protein atoms included.^[55] Next, the CHARMM-GUI environment was used for protein manipulation and construction of the solvated complexes of MurD protein with compounds 8 and 12.^[57] The CHARMM parameter and topology files (version 27) were used to specify the force field parameters of the amino acid residues comprising the MurD protein.^[58,59] The CHARMM general force field (CGenFF) was used to describe the atom types and partial charges of compounds 8 and 12.^[60] Determined partial charges and assigned atom types for both compounds are listed in the Supporting Information (Tables S3 and S4). The protein–ligand system was immersed in a TIP3 sphere of water molecules^[61] with a truncated octahedral shape with edge distances of 10 Å, and six chlorine ions were added to make the system electroneutral. Ion placement was performed using the Monte Carlo method. The periodic boundary conditions (PBC) were applied based on the shape and size of the system. Grid information for particle-mesh Ewald (PME) fast Fourier transform (FFT) was gen-

erated automatically. The final systems prepared for the MD simulation were comprised of 73,287 and 72,347 atoms. Short steps of energy minimization were then performed to remove bad contacts. Three systems were then minimized for 2000 steps using steepest descent (SD) method followed by 2000 steps of the modified Adopted Basis Newton-Raphson (ABNR) method and an MD equilibration run of 350 ps.

These production MD trajectories were generated using the Leapfrog integration scheme and a 2 fs simulation step using the SHAKE algorithm. A 10 ns MD simulation production run was performed. Conformations were sampled every 100th step, resulting in 5000 conformations for subsequent analysis. Visualization and analysis of the geometry parameters of the production MD trajectories were performed using the VMD program.^[62] Further inspection of the overall conformational behavior for each MD simulation can also be seen in the generated movie animations (see Supporting Information).

In vitro screening of selected hit compounds for htlI α inhibitory activity

The assay was performed on black streptavidin-coated 96-well microtiter plates. The plates were rehydrated using wash buffer (20 mM Tris-HCl (pH 7.6), 137 mM NaCl, 0.01 % (w/v) BSA, 0.05 % (v/v) Tween-20), and biotinylated oligonucleotide was immobilized onto the wells. Next, the excess oligonucleotide was removed by washing with wash buffer. The enzyme assay was carried out in a reaction volume of 30 μ L using 0.75 μ g supercoiled plasmid pNO1 as a substrate and 1.5 U of htlI α . Tested compounds (0.3 μ L) were added as stock solutions in DMSO, with a final concentration of 1 % DMSO. Reactions were incubated at 37 °C for 30 min, and TF buffer (50 mM NaOAc (pH 5.0), 50 mM NaCl, 50 mM MgCl₂) was added to the wells and incubated at room temperature for an additional 30 min to allow triplex formation (biotin-oligonucleotide-plasmid).^[44] To eliminate aggregation and non-specific inhibition, a surfactant (Tween-20) was added to the reaction mixture.^[45] Unbound plasmid was removed by washing with TF buffer, and a solution of SybrGOLD stain (Invitrogen) in T10 buffer (10 mM Tris-HCl (pH 8) and 1 mM EDTA) was added. After mixing, fluorescence was read using a Tecan fluorimeter (excitation: 485 nm, emission: 535 nm). Preliminary screening was performed at inhibitor concentrations of 500, 125, 31.3, and 7.8 μ M, and all active compounds were tested at four additional concentrations (250, 62.5, 15.6, and 3.9 μ M).^[44] IC₅₀ values were calculated using GraphPad Prism 6.0 software and represent the concentration of inhibitor at which residual activity of enzyme was 50 %. Results of the inhibition assay for compounds 5, 6, 8, 9, 12–15, and 20–23 are presented in Figure S5.^[44] Independent experiments were repeated twice. Obtained IC₅₀ values are presented in Tables 1 and 2. Commercially available compounds 5, 6, 8, 9, 12–14, and 20–22, possessing htlI α activity, were characterized by HRMS, and their purity was determined by microanalysis using a PerkinElmer C, H, N, S analyzer and a modified Pregl-Dumas method. Analyses indicated that all elements were within 0.5 % of theoretical values. The purities of the tested compounds were established as \geq 95 % (see Supporting Information Section 13).

Determination of IC₅₀ values for DNA gyrase using a standard inhibitory assay

The assay was performed on black streptavidin-coated 96-well microtiter plates. The plates were rehydrated using wash buffer

(20 mM Tris-HCl (pH 7.6), 137 mM NaCl, 0.01 % (w/v) BSA, 0.05 % (v/v) Tween-20). In next step, biotinylated oligonucleotide was immobilized onto the wells, and the excess oligonucleotide was removed by washing with wash buffer. The enzyme assay was carried out in a reaction volume of 30 μ L containing 1 μ g of relaxed pNO1 plasmid as a substrate and 1.5 U of DNA gyrase from *E. coli*. Tested compounds (0.3 μ L) were added as stock solutions in DMSO with a final concentration of 1 % DMSO. Reactions were incubated at 37 °C for 30 min, and TF buffer (50 mM NaOAc (pH 5.0), 50 mM NaCl, 50 mM MgCl₂) was added to the wells and incubated at room temperature for an additional 30 min to allow triplex formation (biotin-oligonucleotide-plasmid).^[44] To eliminate aggregation and non-specific inhibition, a surfactant (Tween-20) was added to the reaction mixture.^[45] Unbound plasmid was removed by washing with TF buffer, and a solution of SybrGOLD stain (Invitrogen) in T10 buffer (10 mM Tris-HCl (pH 8) and 1 mM EDTA) was added. After mixing, fluorescence was read using a Tecan fluorimeter (excitation: 485 nm, emission: 535 nm). Preliminary screening was performed at inhibitor concentrations of 500, 125, 31.3, and 7.8 μ M, and all active compounds were tested at four additional concentrations (250, 62.5, 15.6, and 3.9 μ M).^[44] IC₅₀ values were calculated using GraphPad Prism 6.0 software and represent the concentration of inhibitor at which residual activity of enzyme was 50%.^[44] Results are presented in Table 1.

Human DNA topoisomerase II α decatenation assay

The htlI α decatenation assay was performed in collaboration with Inspiralis (Norwich, UK). A decatenation assay kit from Inspiralis was used to determine the effect of compounds **8** and **12** on DNA decatenation; 1 U of htlI α was incubated with 200 ng kDNA in a 30 μ L reaction at 37 °C for 30 min under the following conditions: 50 mM Tris-HCl (pH 7.5), 125 mM NaCl, 10 mM MgCl₂, 5 mM DTT, 0.5 mM EDTA, 0.1 mg mL⁻¹ bovine serum albumin (BSA), and 1 mM ATP. The final DMSO concentration in all the reactions was 1 % (v/v). Compounds were serially diluted in DMSO and added to the reaction before the addition of enzyme. Etoposide (**1**) was used as a control compound. Each reaction was stopped by the addition of 30 μ L chloroform/isoamyl alcohol (26:1) and 30 μ L Stop Dye before being loaded on a 1 % TAE gel and run at 85 V for 90 min. Experiments were run in duplicate for both compounds. Bands were visualized by ethidium bromide staining for 15 min and destaining for 10 min. Gels were scanned using documentation equipment (GeneGenius, Syngene, Cambridge, UK), and inhibition levels were calculated from band data obtained with gel scanning software (GeneTools, Syngene, Cambridge, UK).

SPR experiments

Surface plasmon resonance (SPR) experiments were performed at 25 °C using a BiacoreX (Biacore, GE Healthcare) instrument. The system was primed twice with running buffer (10 mM HEPES pH 7.4, 150 mM NaCl, 3 mM EDTA, 0.005 % surfactant P20). Using a standard amino coupling method, htlI α ATPase was immobilized on the second flow cell of a CM5 sensor chip. The htlI α ATPase domain (fragment containing residues 1–453 with a His tag) was purchased from Inspiralis.^[63] The carboxymethylated dextran layer was activated with a 7 min pulse of EDC (1-ethyl-3-(3-dimethylethylaminopropyl)-carbodiimide) and NHS (N-hydroxysuccinimide) in a 1:1 ratio. HtlI α ATPase, diluted to a final concentration of 50 μ g mL⁻¹ in 10 mM sodium acetate (pH 5.5), was injected in two short pulses to reach a final immobilization level around 16 000 response units. The rest of the surface was deactivated with a 7 min

injection of ethanolamine. The first flow served as a reference cell for subtraction of nonspecific binding and was activated with EDC/NHS and deactivated with ethanolamine. The system was reprimed with new running buffer (10 mM HEPES pH 7.4, 150 mM NaCl, 3 mM EDTA, 0.005 % surfactant P20). Analytes were prepared as 100 \times stock solutions in DMSO and were diluted with running buffer (10 mM HEPES pH 7.4, 150 mM NaCl, 3 mM EDTA, 0.005 % surfactant P20). Analytes were injected at a flow rate of 30 μ L min⁻¹ for 60 seconds, and dissociation was monitored for an additional 30 seconds.^[47] To diminish the difference in the refractive index between samples and running buffer for the titration of analytes, 1 % (v/v) DMSO (2 μ L 100 % DMSO) was added to the running buffer (198 μ L). Analytes were tested in at least eight different concentrations in three parallel titrations. Some concentrations were injected several times to check reproducibility. Sensorgrams were analyzed using BIAeval software (Biacore, GE Healthcare). Equilibrium binding responses were determined from the binding levels 5 sec before stopping the injections, and finally, K_D values were determined using Origin 6.1 software by fitting the data to 1:1 steady-state binding models.

In vitro cytotoxicity measurements (MTT assay)

The in vitro cytotoxicities of active compounds **5**, **6**, **8**, **9**, **12–14**, and **20–22** were evaluated against two human cancer cell lines—MCF-7 (breast cancer) and HepG2 (hepatoma)—and against HUVEC cells (human endothelial cells), which represent normal cells in the 3-(4,5-dimethylthiazol-2-yl)-2,5-diphenyltetrazolium bromide (MTT) assay, according to Mosmann,^[64] with minor modifications.^[65] HepG2 cells (provided by Prof. F. Darroudi from Leiden University Medical Centre, Department of Toxicogenetics, Leiden, The Netherlands) were cultivated in William's medium E (W-1878, Sigma), and MCF-7 (ATCC) and HUVEC (ECACC) were cultivated in Eagle's MEM medium. All media were supplemented with 10 % fetal bovine serum, 2 mM glutamine, and 100 U mL⁻¹ penicillin/streptomycin. The cells were incubated at 37 °C in humidified atmosphere with 5 % CO₂.

The cells were seeded onto 96-well microplates at densities of 9000 cells per well (HepG2) and 7000 cells per well (HUVEC and MCF-7) in 200 μ L growth medium and incubated overnight to attach. The next day, the growth medium was replaced by fresh complete growth medium containing appropriate concentrations of the test compounds. Prepared microplates were then incubated for an additional 24 h. In each experiment, a vehicle control (1 % DMSO) and a positive control (etoposide, 40 μ M concentration) were included. After incubation, 20 μ L of MTT reagent was added to each well, and the plates were incubated for an additional 3 h. The medium was then removed, and the resulting formazan crystals were dissolved in 200 μ L of DMSO. The amount of formazan crystals directly correlates to the number of viable cells. The optical density (OD) of the wells was measured at 570 nm (reference filter 690 nm) using a GENios microplate spectrofluorimeter (Tecan, Trappes, France). Cell viability was determined by comparing the OD of the wells containing the cells treated with test compounds to those with the vehicle control. Independent experiments were performed in five replicates and were repeated three times.

Data analysis and statistical evaluation

Statistical significance between treated groups and the vehicle control was determined by a two-tailed Student's *t* test, and *P* < 0.01 was considered significant. In addition, we calculated the stat-

istical significance between the non-cancer HUVEC cell line and cancer cell lines (HepG2 and MCF-7) using GraphPad Prism 6.0 (GraphPad Software). EC₅₀ values were determined by nonlinear regression using a dose–response equation of surviving cells after exposure to compounds. The EC₅₀ value is the concentration of inhibitor that gives a half-maximal response 50%.^[66]

Abbreviations

AMP-PNP, 5'-adenylyl-β,γ-imidodiphosphate; CDK, cyclin-dependent kinase; DMSO, dimethyl sulfoxide; EA, ethanolamine; ECACC, European Collection of Cell Cultures; EDC, 1-ethyl-3-(3-dimethylethylaminopropyl)-carbodiimide; EDTA, ethylenediaminetetraacetic acid; FLD, flow linear dichroism; GA, genetic algorithm; GHKL, DNA gyrase, Hsp90, histidine kinase, and MutL; HepG2, human hepatocellular carcinoma cell line; HEPES, 4-(2-hydroxyethyl)-1-piperazineethanesulfonic acid; HUVEC, human umbilical vein endothelial cells; htlIβ, human topoisomerase IIβ; htlIα, human topoisomerase IIα; kDNA, kinetoplast; LE, ligand efficiency; MCF-7, human breast cancer cell line; MD, molecular dynamics; MTT, 3-(4,5-dimethylthiazol-2-yl)-2,5-diphenyltetrazolium bromide; NHS, N-hydroxysuccinimide; PC, positive control; SPR, surface plasmon resonance; topo, topoisomerase; TPSA, topological surface area; vdW, van der Waals energy; QTK loop, glutamine-threonine-leucine loop.

Supporting Information

1) 3D structure-based pharmacophore of the AMP-PNP molecule; 2) 3D structure-based pharmacophore with aligned inactive molecules; 3) GOLD molecular docking tool validation; 4) Comparison of docked AMP-PNP (4) and compounds 5 and 8; 5) Results of inhibition assay for compounds 5, 6, 8, 9, 12–15, and 20–23; 6) GOLD-calculated binding model of the inactive virtual screening hits 18 and 29; 7) Results of htlIα-mediated decatenation assay; 8) SPR sensorgram and calculated K_D value for reference compound etoposide (1); 9) Calculated K_D values for compounds 8 and 12; 10) Partial charges and atom types for simulated compound 8 and 12; 11) Measured time-dependent distances between selected protein atoms and compounds 8 and 12; 12) Complete list of tested compounds; 13) Analytical and spectral characterization data; 14) Complete and ligand-enlarged animations of the production stage MD simulations of compounds 8 and 12.

Acknowledgements

This work was supported by the Ministry of Education, Science, and Sport of the Republic of Slovenia through Young Researcher Grant 1000-10-310260 to B.P., Postdoctoral Grant Z1-4111 to A.P., and Research Program Grant P1-0012 to B.P., A.P., and T.S. The authors sincerely thank and acknowledge Prof. Gregor Anderluh from the National Institute of Chemistry in Ljubljana for helpful discussions concerning SPR measurements and Vesna Hodnik from the Department for Biology, Biotechnical Faculty, Ljubljana for technical assistance with these experiments. The authors also thank Džejla Bajrektarević from the National Institute of Biology, Department of Genetic Toxicology and Cancer Biology, Ljubljana for her assistance with cytotoxicity measurements. The authors acknowledge Drs. Nicolas Burton and Alison Howells from Inspiralis, Norwich, UK for performing the human DNA topoisomerase

IIα decatenation assay. Matej Janežič is thanked for technical assistance with the analysis of MD trajectories.

Keywords: anticancer agents • catalytic inhibitors • human DNA topoisomerase IIα • MTT assay • virtual screening

- [1] K. R. Hande, *Biochim. Biophys. Acta Gene Struct. Expression* **1998**, *1400*, 173–184.
- [2] A. D. Bates, A. Maxwell, *Curr. Biol.* **1997**, *7*, R778–R781.
- [3] J. J. Champoux, *Annu. Rev. Biochem.* **2001**, *70*, 369–413.
- [4] A. J. Schoeffler, J. M. Berger, *Q. Rev. Biophys.* **2008**, *41*, 41–101.
- [5] B. Pogorelčnik, A. Perdih, T. Solmajer, *Curr. Pharm. Des.* **2013**, *19*, 2474–2488.
- [6] B. Pogorelčnik, A. Perdih, T. Solmajer, *Curr. Med. Chem.* **2013**, *20*, 694–709.
- [7] E. L. Baldwin, N. Osheroff, *Curr. Med. Chem. Anticancer Agents* **2005**, *5*, 363–372.
- [8] G. Minotti, P. Menna, E. Salvatorelli, G. Cairo, L. Gianni, *Pharmacol. Rev.* **2004**, *56*, 185–229.
- [9] E. M. Nelson, K. M. Tewey, L. F. Liu, *Proc. Natl. Acad. Sci. USA* **1984**, *81*, 1361–1365.
- [10] D. C. Case, T. J. Ervin, M. A. Boyd, L. G. Bove, H. L. Sonneborn, S. D. Paul, *Am. J. Clin. Oncol.* **1987**, *10*, 523–526.
- [11] R. P. McGeary, A. J. Bennett, Q. B. Tran, K. L. Cosgrove, B. P. Ross, *Mini-Rev. Med. Chem.* **2008**, *8*, 1384–1394.
- [12] J. M. Fortune, N. Osheroff, *J. Biol. Chem.* **1998**, *273*, 17643–17650.
- [13] T. Andoh, *Biochimie* **1998**, *80*, 235–246.
- [14] P. Furet, J. Schoepfer, T. Radimerski, P. Chene, *Bioorg. Med. Chem. Lett.* **2009**, *19*, 4014–4017.
- [15] M. Brvar, A. Perdih, M. Renko, G. Anderluh, D. Turk, T. Solmajer, *J. Med. Chem.* **2012**, *55*, 6413–6426.
- [16] M. Brvar, A. Perdih, V. Hodnik, M. Renko, G. Anderluh, R. Jerala, T. Solmajer, *Bioorg. Med. Chem.* **2012**, *20*, 2572–2580.
- [17] M. Brvar, A. Perdih, M. Oblak, L. P. Masic, T. Solmajer, *Bioorg. Med. Chem. Lett.* **2010**, *20*, 958–962.
- [18] K. D. Corbett, J. M. Berger, *Annu. Rev. Biophys. Biomol. Struct.* **2004**, *33*, 95–118.
- [19] P. Chène, *Nat. Rev. Drug Discovery* **2002**, *1*, 665–673.
- [20] R. Dutta, M. Inouye, *Trends Biochem. Sci.* **2000**, *25*, 24–28.
- [21] H. Wei, A. J. Ruthenburg, S. K. Bechis, G. L. Verdine, *J. Biol. Chem.* **2005**, *280*, 37041–37047.
- [22] S. Bendsen, V. H. Oestergaard, C. Skouboe, M. Brinch, B. R. Knudsen, A. H. Andersen, *Biochemistry* **2009**, *48*, 6508–6515.
- [23] P. Chène, J. Rudloff, J. Schoepfer, P. Furet, P. Meier, Z. Qian, J. M. Schlaeppli, R. Schmitz, T. Radimerski, *BMC Chem. Biol.* **2009**, *9*, 1.
- [24] L. H. Jensen, H. Liang, R. Shoemaker, M. Grauslund, M. Sehested, B. B. Hasinoff, *Mol. Pharmacol.* **2006**, *70*, 1503–1513.
- [25] L. H. Jensen, A. V. Thougard, M. Grauslund, B. Sokilde, E. V. Carstensen, H. K. Dvinge, D. A. Scudiero, P. B. Jensen, R. H. Shoemaker, M. Sehested, *Cancer Res.* **2005**, *65*, 7470–7477.
- [26] V. Gandhi, M. Ayres, R. G. Halgren, N. L. Krett, R. A. Newman, S. T. Rosen, *Cancer Res.* **2001**, *61*, 5474–5479.
- [27] A. T. Baviskar, C. Madaan, R. Preeth, P. Mohapatra, V. Jain, A. Agarwal, S. K. Guchhait, C. N. Kundu, U. C. Banerjee, P. V. Bharatam, *J. Med. Chem.* **2011**, *54*, 5013–5030.
- [28] B. Pogorelčnik, M. Brvar, I. Zajc, M. Filipič, T. Solmajer, A. Perdih, *Bioorg. Med. Chem. Lett.* **2014**, *24*, 5762–5768.
- [29] H. Huang, Q. Chen, X. Ku, L. H. Meng, L. P. Lin, X. Wang, C. H. Zhu, Y. Wang, Z. Chen, M. Li, H. L. Jiang, K. X. Chen, J. Ding, H. Liu, *J. Med. Chem.* **2010**, *53*, 3048–3064.
- [30] K. Y. Jun, E. Y. Lee, M. J. Jung, O. H. Lee, E. S. Lee, H. Y. P. Choo, Y. Na, Y. Kwon, *Eur. J. Med. Chem.* **2011**, *46*, 1964–1971.
- [31] Y. Ma, J. G. Wang, B. Wang, Z. M. Li, *J. Mol. Model.* **2011**, *17*, 1899–1909.
- [32] B. Wang, Z. W. Miao, J. Wang, R. Y. Chen, X. D. Zhang, *Amino Acids* **2008**, *35*, 463–468.
- [33] M. Gui, D. K. Shi, M. Huang, Y. Zhao, Q. M. Sun, J. Zhang, Q. Chen, J. M. Feng, C. H. Liu, M. Li, Y. X. Li, M. Geng, J. Ding, *Invest. New Drugs* **2011**, *29*, 800–810.

- [34] C. X. Hu, Z. L. Zuo, B. Xiong, J. G. Ma, M. Y. Geng, L. P. Lin, H. L. Jiang, J. Ding, *Mol. Pharmacol.* **2006**, *70*, 1593–1601.
- [35] Y. Qin, L. Meng, C. Hu, W. Duan, Z. Zuo, L. Lin, X. Zhang, J. Ding, *Mol. Cancer Ther.* **2007**, *6*, 2429–2440.
- [36] M. Li, Z. H. Miao, Z. Chen, Q. Chen, M. Gui, L. P. Lin, P. Sun, Y. H. Yi, J. Ding, *Ann. Oncol.* **2010**, *21*, 597–607.
- [37] P. Wang, C. H. Leung, D. L. Ma, W. Lu, C. M. Che, *Chem. Asian J.* **2010**, *5*, 2271–2280.
- [38] A. Perdih, A. Kovac, G. Wolber, D. Blanot, S. Gobec, T. Solmajer, *Bioorg. Med. Chem. Lett.* **2009**, *19*, 2668–2673.
- [39] G. Wolber, T. Langer, *J. Chem. Inf. Model.* **2005**, *45*, 160–169.
- [40] eMolecules virtual compound screening database: www.emolecules.com.
- [41] G. Jones, P. Willett, R. C. Glen, A. R. Leach, R. Taylor, *J. Mol. Biol.* **1997**, *267*, 727–748.
- [42] G. L. Chen, L. Yang, T. C. Rowe, B. D. Halligan, K. M. Tewey, L. F. Liu, *J. Biol. Chem.* **1984**, *259*, 13560–13566.
- [43] W. B. Wu, J. B. Ou, Z. H. Huang, S. B. Chen, T. M. Ou, J. H. Tan, D. Li, L. L. Shen, S. L. Huang, L. Q. Gu, Z. S. Huang, *Eur. J. Med. Chem.* **2011**, *46*, 3339–3347.
- [44] A. Maxwell, N. P. Burton, N. O'Hagan, *Nucleic Acids Res.* **2006**, *34*, e104.
- [45] A. J. Ryan, N. M. Gray, P. N. Lowe, C. W. Chung, *J. Med. Chem.* **2003**, *46*, 3448–3451.
- [46] P. C. D. Hawkins, A. G. Skillman, G. L. Warren, B. A. Ellingson, M. T. Stahl, *J. Chem. Inf. Model.* **2010**, *50*, 572–584.
- [47] N. J. de Mol, M. J. Fischer, *Methods Mol. Biol.* **2010**, *627*, 1–14.
- [48] R. Rich, D. Myszk, *J. Mol. Recognit.* **2010**, *23*, 392–392.
- [49] A. Gabibov, E. Yakubovskaya, M. Lukin, P. Favorov, A. Reshetnyak, M. Monastyrsky, *FEBS J.* **2005**, *272*, 6336–6343.
- [50] A. Perdih, G. Wolber, T. Solmajer, *J. Comput.-Aid. Mol. Des.* **2013**, *27*, 723–738.
- [51] B. R. Brooks, R. E. Bruccoleri, B. D. Olafson, D. J. States, S. Swaminathan, M. Karplus, *J. Comput. Chem.* **1983**, *4*, 187–217.
- [52] C. Abad-Zapatero, *Expert Opin. Drug Discovery* **2007**, *2*, 469–488.
- [53] V. Škedelj, A. Perdih, M. Brvar, A. Kroflič, V. Dubbée, V. Savage, A. J. O'Neill, T. Solmajer, M. Bešter-Rogač, D. Blanot, J. E. Hugonnet, S. Magnet, M. Arthur, J. L. Mainardi, J. Stojan, A. Zega, *Eur. J. Med. Chem.* **2013**, *67*, 208–220.
- [54] J. Kirchmair, P. Markt, S. Distinto, G. Wolber, T. Langer, *J. Comput.-Aid. Mol. Des.* **2008**, *22*, 213–228.
- [55] C. Azuara, E. Lindahl, P. Koehl, H. Orland, M. Delarue, *Nucleic Acids Res.* **2006**, *34*, W38–W42.
- [56] D. Hoffmann, E. W. Knapp, *Phys. Rev. E* **1996**, *53*, 4221–4224.
- [57] S. Jo, T. Kim, V. G. Iyer, W. Im, *J. Comput. Chem.* **2008**, *29*, 1859–1865.
- [58] A. D. MacKerell, D. Bashford, M. Bellott, R. L. Dunbrack, J. D. Evanseck, M. J. Field, S. Fischer, J. Gao, H. Guo, S. Ha, D. Joseph-McCarthy, L. Kuchnir, K. Kucera, F. T. K. Lau, C. Mattos, S. Michnick, T. Ngo, D. T. Nguyen, B. Prodhom, W. E. Reiher, B. Roux, M. Schlenkrich, J. C. Smith, R. Stote, J. Straub, M. Watanabe, J. Wiorkiewicz-Kuczera, D. Yin, M. Karplus, *J. Phys. Chem. B* **1998**, *102*, 3586–3616.
- [59] A. D. Mackerell, M. Feig, C. L. Brooks, *J. Comput. Chem.* **2004**, *25*, 1400–1415.
- [60] K. Vanommeslaeghe, E. Hatcher, C. Acharya, S. Kundu, S. Zhong, J. Shim, E. Darian, O. Guvench, P. Lopes, I. Vorobyov, A. D. MacKerell, Jr., *J. Comput. Chem.* **2010**, *31*, 671–690.
- [61] W. L. Jorgensen, J. Chandrasekhar, J. D. Madura, R. W. Impey, M. L. Klein, *J. Chem. Phys.* **1983**, *79*, 926–935.
- [62] W. Humphrey, A. Dalke, K. Schulten, *J. Mol. Graph. Model.* **1996**, *14*, 33–38.
- [63] S. Campbell, A. Maxwell, *J. Mol. Biol.* **2002**, *320*, 171–188.
- [64] T. Mosmann, *J. Immunol. Methods* **1983**, *65*, 55–63.
- [65] B. Zegura, I. Zajc, T. T. Lah, M. Filipič, *Toxicol.* **2008**, *51*, 615–623.
- [66] P. Brezovšek, T. Eleršek, M. Filipič, *Water Res.* **2014**, *52*, 168–177.

Received: October 22, 2014

Published online on December 17, 2014